HHS Public Access

Author manuscript

Biochimie. Author manuscript; available in PMC 2022 December 01.

Published in final edited form as:

Biochimie. 2021 December ; 191: 104–117. doi:10.1016/j.biochi.2021.09.003.

Uncovering a delicate balance between endonuclease RNase III and ribosomal protein S15 in *E. coli* ribosome assembly

Anusha Naganathan[a], **Roxanne Keltz**[a], **Hiram Lyon**[a], **Gloria M. Culver**[a,b,c]

[a]Department of Biology, University of Rochester, Rochester, NY, USA

[b]Center for RNA Biology, University of Rochester, Rochester, NY, USA

[c]Department of Biochemistry and Biophysics, University of Rochester, Rochester, NY, USA

Abstract

The bacterial ribosomal protein S15 is located in the platform, a functional region of the 30S ribosomal subunit. While S15 is critical for *in vitro* formation of *E. coli* small subunits (SSUs), it is dispensable for *in vivo* biogenesis and growth. In this work, a novel synergistic interaction between *rpsO*, the gene that encodes S15, and *rnc* (the gene that encodes RNase III), was uncovered in *E. coli*. RNase III catalyzes processing of precursor ribosomal RNA (rRNA) transcripts and thus is involved in functional ribosome subunit maturation. Strains lacking S15 (*ΔrpsO*), RNase III (*Δrnc*) or both genes were examined to understand the relationship between these two factors and the impact of this double deletion on rRNA processing and SSU maturation. The double deletion of *rpsO* and *rnc* partially alleviates the observed cold sensitivity of *ΔrpsO* alone. A novel 16S rRNA precursor (17S* rRNA) that is detected in in free 30S subunits of *Δrnc* is incorporated in 70S-like ribosomes in the double deletion. The stable accumulation of 17S* rRNA suggests that timing of processing events is closely coupled with SSU formation events *in vivo*. The double deletion has a suppressive effect on the cell elongation phenotype of *ΔrpsO*. The alteration of the phenotypes associated with S15 loss, due to the absence of RNase III, indicates that pre-rRNA processing and improvement of growth, relative to that observed for *ΔrpsO*, are connected. The characterization of the functional link between the two factors illustrates that there are redundancies and compensatory pathways for SSU maturation.

Keywords

ribosome; biogenesis; 16S rRNA; 17S rRNA; RNase III; S15; E. coli

anaganat@ur.rochester.edu, Gloria.culver@rochester.edu, Address: 301 Hutchinson Hall University of Rochester Rochester, NY 14627, Phone: +1 (585)-276-2372.

AUTHOR CONTRIBUTIONS:

A.N and G.M.C conceived and designed the experiments. A.N, R.K, and H.L conducted experiments and collected the data, A.N. performed the analysis, A.N and G.M.C wrote the manuscript. All authors have approved the final article. The authors have no competing interests to declare.

1. Introduction:

The ribosome is a universally conserved machine that carries out the crucial process of translation. Ribosomal rRNA (rRNA) forms the catalytic core of the ribosome, while ribosomal proteins (r-proteins) provide structural scaffolding for efficient rRNA folding, tertiary structure formation, and changes to fidelity and accuracy [1, 2]. Prokaryotic ribosome biogenesis has emerged as an attractive antibacterial target; some antibiotics have been shown to directly bind to precursor ribosomal subunits and alter biogenesis and growth [3–5]. To date, it is still difficult to separate the effects of these antibiotics on the process of translation versus the process of subunit biosynthesis [5, 6]. Thus, a deeper understanding of the prokaryotic ribosomal subunit biogenesis cascade *in vivo* is crucial to dissecting and identifying antibiotic resistance mechanisms (via separation of function) and novel targets for antimicrobials [2, 7, 8]. The production of mature *E. coli* small subunits (SSUs), containing 16S rRNA and 21 r-proteins, requires that the pre-rRNA transcripts undergo a series of rRNA folding, modification, and cleavage events [1, 9–11]. The timing and substrate requirements for these modification and processing events are some of the least understood aspects of prokaryotic ribosome biogenesis.

Emerging evidence from our group and others suggests that multiple pathways can be used during pre-SSU intermediate maturation into functional 30S subunits [12–14]. The pre-SSU rRNA is transcribed as part of a longer transcript containing other functional RNAs (23S rRNA, 5S rRNA, and tRNAs). Soon after or during transcription of the operon such that the full-length 16S rRNA and flanking regions have been synthesized, it is generally observed that RNase III, an endoribonuclease, cleaves the primary transcript when the regions flanking the mature 16S rRNA sequence folds into a double-stranded structure [15, 16]. This cleavage releases 17S rRNA, a precursor of 16S rRNA (Figure 1.B) [9], which contains 5’ leader (115 nucleotides) and a 3’ trailer (33 nucleotides) sequences appended to 16S rRNA (see Figure 3.C). These additional sequences are ultimately processed by other nucleases to produce mature length 16S rRNA [9, 15, 17–19] (Figure 1.B). This *in vivo* cleavage of pre-rRNA appears to occur concurrent with r-protein binding, folding, and modification events [1, 9, 10]. Given the multifaceted processing, a large number of component parts, and the existence of multiple pathways, there is still much to be understood about this process and the relevant components.

Bacterial RNase III is likely the best studied of the nucleases involved in pre-rRNA processing [20], and the catalytic domain of RNase III, which cleaves double-stranded RNA, is found in proteins across all domains of life [21]. Eukaryotic proteins containing the RNase III domain (RIIIDs) are present in key post-transcriptional regulatory factors like Drosha and Dicer [22]. They also play a role in the biogenesis of critical small interfering RNA (siRNA) and microRNA (miRNA), which are effectors of RNA silencing [20]. A richer understanding of the function of RNase III in bacterial ribosome biogenesis could inform our understanding of how these proteins work across the phylogenetic spectrum.

Pre-rRNA maturation events appear to occur simultaneously with the binding of r-proteins [11, 13, 23–25]. Although most small subunit r-proteins appear to play a role in assembly of SSUs using mature 16S rRNA *in vitro* [26], *in vivo*, not all 21 SSU r-proteins are essential to

produce functional SSUs [10]. Viable *E. coli* strains have been constructed containing single deletions of genes encoding SSU r-proteins S6, S9, S13, S15, S17, and S20 [23, 25, 27]. The phenotypic consequences to strains that carry these gene deletions are related yet variable [20]. For example, deletion of *rpsF* (S6) in *E. coli* results in an increase in free SSUs and large subunits (LSUs) as well as tolerance for growth under high salt conditions [27]. The deletion of *rpsO* (S15) results in severe cold-sensitivity, SSU maturation delays [24, 28], and a cell elongation phenotype (this study). Given these multiple phenotypes associated with deletion of *rpsO* [24], it is important to gain a further understanding of the roles of the *rpsO* gene product including genetic and functional interactions, and mechanisms that allow for cell viability when *rpsO* is deleted.

In this study, we present evidence to link r-protein S15 and endoribonuclease, RNase III. The work to explore this interaction begins to shed light on the integration of pre-rRNA processing and the broader SSU biogenesis cascade and SSU function. We report that the absence of the *rnc* (RNase III) gene alleviates known growth and some ribosomal defects associated with the *ΔrpsO* strain. The characterization of the RNase III deletion strain also revealed a novel, previously uncharacterized pre-16S rRNA species that is longer than 17S rRNA (named 17S* rRNA herein) and is detected in free subunits and 70S ribosomes. Here the inter-dependency between RNase III and S15 in *E. coli* is characterized, and these data add to our understanding of rRNA processing and the complexity of SSU biosynthesis.

2. Results:

2.1. The absence of S15 severely impairs 16S rRNA maturation and causes ribosome deficiency.

Cold-sensitivity is a hallmark phenotype of strains that are defective in ribosome biogenesis [10, 29, 30]. We observed that the fitness of the *ΔrpsO* strain was considerably reduced compared to *wild-type E. coli* at standard growth temperature of 37°C (Figure 2.A, *wild-type: cross marks* and *ΔrpsO: open circles*). As previously reported, [24, 28], *ΔrpsO* is viable but exhibits extreme cold-sensitivity (Figure 2.A, *right*). In earlier work, primer extension analysis revealed the presence of a precursor 16S rRNA in free SSUs in the *ΔrpsO* strain [28]. To investigate, in a more quantitative manner, the effect of S15 on SSU maturation, 30S subunits were fractionated from *wild-type* and *ΔrpsO* strains, rRNA was extracted, and then analyzed by northern blotting (Figure 2.B). SSU ribosomal peaks were collected in three contiguous fractions (as described in Materials and Methods) and the isolated RNA was probed using primers for leader (5'), trailer (3'), and the mature regions of 16S rRNA. In Figure 2.B, fraction 2 represents the apex of the fractionated 30S subunit peak (see Figure S3 for labeled ribosome profiles). The presence of bands detected with both the leader and trailer probes indicates the presence of 17S rRNA (Figure 2.B). At 37°C, increased accumulation of 17S rRNA was observed in *ΔrpsO* SSUs compared to SSUs isolated from the *wild-type* strain (Figure 2.B**, leader and trailer probes**). The amount of 17S rRNA was notably increased at lower temperature (25°C) and in *ΔrpsO* SSUs compared to *wild-type* SSUs grown under the same conditions. The relative amounts of 17S/16S rRNA in 30S subunits was quantified by densitometry (see Materials and Methods). At 25°C, the *ΔrpsO* 30S subunits contain over ~30-fold more 17S rRNA and a decreased fraction of

mature 16S rRNA relative to the *wild-type* counterparts (Figure 2.C). These data suggest that ribosome biogenesis delays are exacerbated and the formation of mature 16S rRNA is severely affected in *ΔrpsO* at low temperature.

In *ΔrpsO*, a significant deficiency of 70S ribosomes was observed compared to *wild-type* at both temperatures (Figure S4). 17S rRNA could not be detected in these 70S-like ribosomal fractions by northern blotting (data not shown), but the presence of 17S rRNA in 70S-like fractions was characterized using modified 3'-5' RACE [20] and is discussed in detail in this study (Figure 6 and Figure 7). These analyses reveal that *ΔrpsO* not only leads to a marked 70S deficiency, but the cold-sensitive phenotype is correlated with exacerbated maturation defects and the accumulation of 17S rRNA-containing 30S subunits in *ΔrpsO*.

2.2. The deletion of RNase III results in the accumulation of a novel precursor SSU rRNA processing intermediate.

RNase III cleavage is one of the first steps in *wild-type* SSU biogenesis, and results in the release of 17S rRNA from the primary transcript [16]; 17S rRNA is subsequently processed to mature 16S rRNA by a variety of enzymes [14, 15, 17–19, 31]. Despite its function in processing precursor rRNA, RNase III is not essential for viability in *E. coli*, and strains lacking the *rnc* gene do not exhibit dramatic growth defects [16, 31]. Additionally, *E. coli* strains bearing a *rnc* deletion are able to form fully mature 16S rRNA (Figure 1.B and Figure 3.B), which is indicative of the high functional redundancy of *E. coli* 16S rRNA processing enzymes [20] and in SSU biogenesis more broadly [12, 13].

While mature 16S rRNA can be formed in the absence of RNase III, the pathway for maturation remains unclear. To investigate how the absence of RNase III might influence SSU biogenesis, rRNA from 30S subunits and 70S ribosomal particles from *Δrnc* were analyzed. The sucrose gradient profiles of *Δrnc* ribosomes did not display any significant difference compared to *wild-type* (Figure S4), indicating that the formation of free ribosomal subunits and assembled 70S ribosomes is not perturbed in this strain (Figure 3.A). The rRNA isolated from the ribosomal peaks was analyzed using modified 3' to 5' RACE [20] to reveal 16S rRNA-containing species. Interestingly, we observed a novel, immature rRNA species, longer than 17S rRNA in 30S subunits formed in *Δrnc* grown at 25°C (called **17S* rRNA** here) (Figure 3.B and 3.C). TOPO-TA cloning of RACE products [14] (see Materials and Methods) and subsequent sequencing revealed that 17S* rRNA contains 133 nucleotides upstream of the mature 5' end of 16S rRNA (leader) and 49 nucleotides downstream at the mature 3' end of 16S rRNA (trailer) (Figure 3.B). Thus, this intermediate contains additional sequences at both ends as compared to 17S rRNA (Figure 3.C and Figure S8) and was detected at both temperatures tested (Figure 3.B represents samples from 25°C). This intermediate appears to be the product of cleavage events (and not simply transcription; see Figure S8) as the 5' is shorter than the expected start from either promoter and the end is ligatable as evidence by its detection via RACE. Although precursors longer than 17S rRNA have been observed in a *Δrnc* strain [18, 32], to our knowledge, the 17S* rRNA species has not been reported previously in a *Δrnc* strain or any other strain [16, 32]. It is important to note that this precursor (17S* rRNA) is not detected in the 70S ribosomal fraction in *Δrnc* (Figure 3.B), which could explain the lack of an overt ribosomal abnormality and changes

in growth. The small difference in size between 17S and 17S* rRNA makes it difficult to detect using northern blot analysis and thus could have gone undiscovered. Furthermore, we observed, using both northern blotting and modified 3'-5' RACE, the accumulation of immature 16S rRNA in SSUs from *wild-type* strains grown at low temperature (Figure S5). The accumulation of 17S rRNA in *wild-type* free 30S subunits has been previously reported [18, 33]. However, in comparison to *Δrnc*, we observed that *wild-type* 30S subunits have an enhanced phenotype of immature 16S rRNA accumulation. We were unable to resolve 17S rRNA and 17S* rRNA (the novel species that accumulates in *Δrnc*; see Figure S5.A) via northern blotting. However, using modified 3'-5' RACE we could resolve the immature 16S rRNA species of different lengths and quantify the band intensities (Figure 3.C and Figure S5.B). An increased proportion of mature 16S rRNA, relative to immature 16S rRNA, was observed in 30S subunit fractions from *Δrnc* isolated at 25°C compared to these populations in the parental strain grown under same conditions. This is noteworthy because it suggests that in absence of RNase III, 16S rRNA processing is not thwarted, but instead might proceed unimpeded. However, there are other aspects of 16S rRNA maturation that might be incomplete even if end processing is advanced. The identification of 17S* rRNA is both novel and significant for further characterization of SSU maturation overall and the role of RNase III is this process.

2.3. Cold-sensitivity associated with deletion of *rpsO* is partially suppressed by co-deletion of *rnc.*

Previous proteomic analysis has shown that RNases and biogenesis factors associate preferentially with SSU intermediates relative to mature 30S subunits [13]. Initial observations using mass spectrometry (LC-MS/MS; two technical replicates for each strain and temperature), we observed that some RNases were differentially detected in *ΔrpsO* SSUs at both temperatures compared to *wild-type* SSUs at the same temperatures (Supplemental Table 1 and 2; see Materials and Methods). This pattern of association of ribonucleases with *ΔrpsO* SSUs led us to explore potential functional interactions between S15 and RNases involved in 16S rRNA processing. Because the mass spectrometry data were not from biological replicates and thus were only suggestive, we took a genetic approach to create double deletions of some of the ribonucleases detected by mass spectrometry (RNase G - *ΔrngΔrpsO*, RNase R – *ΔrnrΔrpsO*, RNase II - *ΔrnbΔrpsO* and RNase III - *ΔrncΔrpsO*). We found that the cold-sensitive phenotype of *ΔrpsO* was not altered upon deletion of these ribonucleases (data not shown), except in the case of RNase III. The phenotype of the double deletion, *ΔrncΔrpsO* is described below.

The gene coding for RNase III (*rnc*) was deleted from *ΔrpsO* and its parental strain. The growth of four strains - *wild-type*, *Δrnc*, *ΔrpsO*, and *ΔrncΔrpsO* - was compared (Figure 4.A and 4.B). The deletion of *rnc* exacerbates the slow growth effect of *ΔrpsO* at 37°C (Figure 4.A *left plate*). Intriguingly, at lower temperature, the deletion of *rnc* in the *ΔrpsO* background mildly suppressed the growth defect of *ΔrpsO* (Figure 4.A *right plate*). The growth curves reveal a slight growth defect in the absence of *rnc* that is noticeable only in liquid culture and the growth defect does not worsen at 25°C as seen in *ΔrpsO* (Figure 4.B). As expected, *ΔrpsO* displays reduced growth compared *to wild-type* and *Δrnc* at 37°C as well as severe cold-sensitivity. The double deletion (*ΔrncΔrpsO*) exhibits

marginally improved fitness at lower temperature. In liquid culture, this is best evident after approximately 20 hours of growth (Figure 4.B**, right**). The absence of RNase III appears to be slightly beneficial to growth of *ΔrpsO* at low temperature. In order to confirm that the suppression conferred by the deletion of *rnc* is not strain-dependent or due to spontaneous mutants, we tested the growth of a second *genetic* background, BW25113 bearing the double deletion [in addition to W3110, the background used for the RNA analysis experiments herein (Figure S2**, liquid media growth and** S6**, solid media growth)].** The results for both backgrounds are very similar and indicate a mild suppression of the *ΔrpsO* growth defect in the absence of *rnc*.

To determine if the presence of RNase III is detrimental under conditions where biogenesis is already delayed (such as low temperature or the absence of S15), we expressed the gene encoding RNase III using an inducible system (pBAD) in *wild-type*, *Δrnc* and *ΔrpsO*. In all backgrounds, the expression of exogenous RNase III results in a distinct growth defect at 37°C but not at 25°C. The 25°C plates were incubated longer (see Materials and Methods) for comparison across all strains, but still no substantial change in growth is observed when RNase III is expressed, compared to the empty vector control, at lower temperature (Figure 4.C).

We observed similar results when comparing growth of these strains in liquid culture (Figure S7). We characterized growth of plasmid-borne cultures (*wild-type: blue, Δrnc: green, ΔrpsO: red*, and *ΔrncΔrpsO: purple*) in the presence of glucose (suppressed, *left*) or arabinose (induced, *right*) at 28°C (see Materials and Methods). The induction of RNase III expression (Figure S7, pBAD-*rnc*, arabinose) leads to decreased growth in all strains, including *Δrnc*, suggesting that exogenous expression of RNase III leads to reduced growth. These data suggest that the level of RNase III is crucial and can have specific impacts on growth.

Conversely, the induction of S15 expression from a vector in a *wild-type* background, with the normal chromosomal copy of *rpsO*, had no impact on growth rates (Figure S7, pBAD-*rpsO*, arabinose). Plasmid-driven S15 expression was able to partially complement growth of the *ΔrpsO* strain, but expression of S15 from the plasmid led to slower growth of *Δrnc* (Figure S7, pBAD-*rpsO*, *green*). Moreover, induction of S15 expression in the absence of *rnc* eliminated the growth advantage afforded by the combined deletion of *rpsO* and *rnc* (Figure S7, pBAD-*rpsO*, *purple*). The improved growth at lower temperature in *ΔrpsO* due to the absence of RNase III indicates that RNase III uniquely impacts 16S rRNA maturation in *ΔrpsO*. Thus, presence of RNase III appears to be disadvantageous under two conditions: - at 37°C (when RNase III expression is driven from an inducible promoter) and in *ΔrpsO* (when RNase III is expressed from its endogenous chromosomal locus). Both genetic states create similar ribosome biogenesis problems indicating the *in vivo* relevance of multiple pathways during SSU biogenesis. The unique phenotypes upon exogenous expression of RNase III and S15 suggests that there is a critical balance between the two factors and their impact on normal SSU biogenesis remains to be investigated.

2.4. A cell elongation phenotype observed in Δ*rpsO* is suppressed by the deletion of *rnc* further supporting a functional interaction between these two loci.

Ribosome biogenesis is a highly coordinated process and changes in the synthesis of mature ribosomes can influence other physiological processes *in vivo* [27, 34, 35]. Growth of *ΔrpsO* at low temperature revealed that this strain was more susceptible to cell lysis compared to the *wild-type* strain grown under the same conditions (see Materials and Methods). To understand this observation, we analyzed cell morphology using phase-contrast microscopy. Cultures from *ΔrpsO* exhibited a highly elongated morphology compared to *wild-type* cultures (Figure 5.A). The absence of S15 leads to a significant increase in cell length (average cell length of *wild-type:* 2.27 μm; *ΔrpsO*: 4.15 μm) (Figure 5.B, *red*). This could explain lysis during growth in liquid culture since longer cells would be more susceptible to lysis via agitation due to shear force action on these cells (Figure 5.A). Other ribosome biogenesis defects have also been associated with an elongated cell phenotype [36, 37]. This phenotype is most easily explained by defective ribosomes formed in the absence of S15 changing cellular functions due to changes in translational capacity and not by another separate role for S15 *in vivo*.

Next, we examined whether the functional interaction observed between RNase III and S15 extended to the cell elongation phenotype. The increase in cell length observed in *ΔrpsO* (4.15 μm) was significantly suppressed in *ΔrncΔrpsO* (2.34 μm) resulting in cell length close to *wild-type* (2.27 μm) (Figure 5.B). Additionally, we observed that the deletion of *rnc* alone leads to a significant decrease in cell length (*Δrnc:* 1.23 μm) (Figure 5.B). Whether the suppression of the *ΔrpsO* growth defect by deletion of *rnc* and the observed decrease in cell length in *Δrnc* are mechanistically related is not clear. However, it is clear that these two gene products impact the same phenotypic outcomes in opposing manners, supporting that *in vivo* a critical balance between the two factors is important.

2.5. RNA analysis of Δ*rnc*Δ*rpsO* (double) reveals a population of 70S ribosomes containing predominantly mature 16S rRNA.

The deletion of the gene encoding S15 results in a significantly reduced growth rate, particularly at low temperatures, 70S deficiency, and a severe SSU rRNA processing defect. Upon comparison of the ribosome profiles of *wild-type* and *Δrnc*, we observed no apparent defects (Figure 3.A), whereas ribosome profiles from both *ΔrpsO* and *ΔrncΔrpsO* showed a significantly reduced proportion of 70S-like particles (Figure 6.A). Moreover, *ΔrncΔrpsO* contained additional peaks in the vicinity of 70S ribosomes (70S-like species) at both temperatures examined. The ribosomal peaks from three independent experiments were used to quantify the percentage of ribosomal subunits and 70S fractions. Figure S4 shows a graphical comparison of the proportion of ribosomal fractions in *wild-type* and *Δrnc* at 37°C and in *ΔrpsO* and *ΔrncΔrpsO* at two different temperatures. The area represented by additional peaks could not be reliably measured for *ΔrpsO* but was consistent enough to be calculated for the double deletion. The significance in differences between ribosomal peaks were tested using Welch's t-test is shown in Figure S4 (Materials and Methods) [38]. There was a significant 70S deficiency observed in *ΔrpsO* and *ΔrncΔrpsO* when compared to *wild-type*. A table of *p values* is provided in Figure S4 and all values less than 0.05 are in red. For analysis, RNA was extracted from each peak observed by sucrose sedimentation

(Figure 6.A) and was subjected to modified 3'-5' RACE analysis (standard modification described in Materials and Methods and as used previously [13, 14]). These RACE analyses result in PCR products, which are products of amplification of different 16S rRNA species, which are discussed herein. For each condition, peak 4 corresponds to the fraction right of the 70S peak (Figure 6.A). The presence of this "second" peak (peak 4) was more prominent in the double deletion compared to the *ΔrpsO* strain (Figure 6.A). The presence of mature and immature 16S rRNA in all fractions was examined by modified 3'-5' RACE (Figure 6.B). In *ΔrpsO*, the peak corresponding to free 30S subunits (peak 1) contained 17S rRNA as well as other immature forms 16S rRNA – which are fully processed at the 3' end but containing immature residues at the 5' end [(a) in Figure 6.B(I)] or are fully processed at the 5' end but contains immature residues at the 3' end [(b) in Figure 6.B(I) and see Figure 3.C **for schematic**]. Strikingly, the SSU fraction of *ΔrncΔrpsO* (peak 1) also contains immature rRNA, but predominantly in form of 17S* rRNA [Figure 6.B (II) and Figure 3.C], Note that peak 2 corresponds to 50S subunits in all samples based on the presence of 23S rRNA (Figure 6.C). Detection of 16S rRNA in the 50S subunit fraction by modified 3'-5' RACE is likely due to the amplification of 16S rRNA contamination from overlapping tails of the adjacent peaks. At both temperatures, "peaks" 3 and 4, from all 4 strains, are 70S populations as they contain 23S rRNA as well as 16S rRNA at roughly appropriate stoichiometry (Figure 6.C). Ribosomal RNA isolated from *ΔrpsO* (peaks 3 and 4) contained partially processed 16S rRNA that resolved between 17S and 16S rRNA bands (labeled (a) and (b)) at both temperatures tested [Figure 6.B(I)]. However, these intermediate species [Figure 3.C; 16S rRNA (a) and (b)] that are processed at either end (but not both) are not detected in *ΔrpsOΔrnc*. Notably, peak 4 from *ΔrncΔrpsO* ribosomal fractionation contained predominantly mature 16S rRNA [along with 23S rRNA (Figure 6.C)] at both temperatures [Figure 6.B (II)]. While 17S* rRNA is clearly detected in the 70S ribosomal fractions (peak 3) in the *ΔrncΔrpsO* deletion, the second population of 70S (peak 4) consists largely of mature 16S rRNA. Thus, unlike *ΔrpsO*, the *ΔrncΔrpsO* contains one predominant immature SSU rRNA – 17S* rRNA. The double deletion also appears to have two distinct populations of 70S ribosome-like particles, one containing predominantly 17S* rRNA and another (to the left of it) containing predominantly fully processed 16S rRNA [Figure 6.A and 6.B(II)].

The appearance of additional 70S-like particles in the double deletion [Figure 6.B(II)] suggests that deletion of *rnc* and thus removal of RNase III may help suppress the defects associated with subunit association [28] and allow formation of 70S ribosomes containing mature rRNA or in 70S-like particles, 17S* rRNA maybe a substrate for further maturation thus producing a sub-population of 70S ribosomes containing mature 16S rRNA. These findings are consistent with suppression of cold-sensitivity associated with *ΔrpsO* by deletion of *rnc*. The highly conserved sequences, across different operons [39], that flank mature 16S rRNA (leader and trailer) are crucial for folding events during SSU maturation [13, 40]. Thus, the absence of *rnc* may slow initial steps in pre-SSU rRNA processing, allowing SSU intermediates formed in the absence of S15 to fold and/or associate with 50S subunits before 17S* rRNA is further cleaved or folded into a structure conducive for further processing.

3. Discussion:

In vitro experiments have shown that S15 is a primary binding ribosomal protein, as it is one of the six SSU proteins to bind directly and independently to 16S rRNA during SSU assembly [26, 30]. The association of S15 with 16S rRNA is required for subsequent binding of specific proteins during the *in vitro* SSU assembly cascade and for the formation of functional SSUs [24]. While indispensable for *in vitro* assembly of *E. coli* 30S subunits, *E. coli* S15 is dispensable for viability *in vivo* [28]. Similarly, RNase III, an endonuclease that cleaves the primary transcript of rRNA early in the processing cascade [9], is also dispensable for growth (Figure 4.A) and strains lacking *rnc* do not have obvious ribosomal defects (Figure 3.A) except the accumulation of a novel intermediate SSU pre-rRNA, 17S* rRNA (Figure 3.B). While readily detectable in 30S subunits, this precursor is not a major component of the assembled 70S ribosomes (Figure 3.B and Figure 7). Changes in fitness and pre-SSU rRNA processing in a strain that lacks both S15 and RNase III, indicates that specific processing events are coupled with different assembly pathways. The highly redundant nature of ribosome biogenesis offers a clear selective advantage over a single pathway or highly funneled cascade.

The 5’ leader and 3’ trailer sequences of 16S rRNA form a double-stranded RNA stem loop which, in the predominant pathway characterized in *wild-type E. coli*, is cleaved by RNase III to release of 17S rRNA from the rest of the primary rRNA transcript that consists of both LSU and SSU rRNA (Figure S1) [41]. These spacer sequences flanking 16S rRNA are highly conserved and play an important role in biogenesis [15, 16]. The 17S rRNA is considered the predominant pre-rRNA of 30S subunits and serves as a scaffold for multiple coordinated events during SSU biogenesis [13, 14]. The region cleaved by RNase III consists of conserved sequences (U3 box A-like sequence) that are known to act in *cis* to chaperone the formation of the SSU central pseudoknot [42], thus supporting the importance of spacer sequences in the step-wise processing and folding of rRNA. We demonstrated using 3’-5’ RACE that a precursor longer than 17S rRNA, 17S* rRNA, accumulates in the absence of RNase III (Figure 3.B). To the best of our knowledge, this 17S* rRNA species has not been identified in previous studies of RNase III-deficient mutants or in other strains, although precursors longer than 17S rRNA have been reported [18, 32]. Hence, its identification is both novel and significant for further characterization of RNase III and S15 function in SSU maturation and to exploring the plasticity of the SSU biogenesis cascade.

The absence of RNase III could briefly (given the lack of impact on doubling times) delay 16S rRNA maturation and thereby create a lag or shift in the biogenesis cascade that is advantageous in the absence of S15. The activity of RNase III influences gene expression at the mRNA level [43]; whether the impact on doubling times and the suppression phenotypes are a direct effect of RNase III’s function in rRNA processing remains to be investigated. However, it is important to note that in the double deletion, free 30S subunits contain 17S* rRNA species while 70S ribosomes appear to contain 17S* rRNA, 17S rRNA, as well as mature 16S rRNA (Figure 6.B (II)). Interestingly, these species were not all present in the same 70S ribosomal population but are distributed in two 70S-like particles (Figure 6.A and Figure 7). These heterogeneous 70S populations indicate a potential suppression mechanism in the *ΔrncΔrpsO* strain that is directly related to RNase III’s function in 16S

rRNA processing. [44]. The presence of a 70S population containing 17S* rRNA suggests that the additional spacer sequences in 17S* rRNA (Figure S8) may allow S15-devoid SSUs to fold better/differently and play a role in biogenesis akin to the role played by the leader and trailer sequences of 17S rRNA [13, 14]. Additionally, a second 70S population containing predominantly mature 16S rRNA suggests that could be the reason for the mild suppression of growth defect in *ΔrncΔrpsO*. Similar to the proposed function of 17S rRNA, 17S* rRNA could also serve as a platform for assembly, especially under cold-sensitive conditions (such as *ΔrpsO* deletion). Such a mechanism could allow the cell to survive the stress of cold-sensitivity by delaying the step-wise processing and accumulating 17S* rRNA-containing SSUs (Figure 7).

It is important to note that there is only a subtle growth advantage of *ΔrncΔrpsO* over *ΔrpsO* at lower temperatures (Figure 4.B). This emphasizes the significant effect that temperature has on ribosome maturation [45]. Whole-cell models of *in vivo* assembly have recently predicted 30S subunit biogenesis intermediates and pathways at high and low temperatures [12]. Kinetic modeling has also shown that S15, along with S4, participates in nucleation events crucial to 30S subunit formation [12]. However, in these models, only 25 percent of 30S subunits were found in active translation, which is different from *in vivo* estimates of over 70 percent [46]. Inclusion of interactions between r-proteins and accessory factors, such as the one discussed herein between S15 and RNase III, will enhance predictions of these *in vivo* processes.

Changes in ribosome biogenesis are evidenced by changes in growth rate as well as protein translation [11, 12, 36, 47]. There is also evidence of the coupling of cell division and ribosome biogenesis in bacteria [48]. Here, we observed an S15-dependent cell elongation phenotype (Figure 5). The cell elongation phenotype of *ΔrpsO* was significantly suppressed in the absence of RNase III. Intriguingly, the single deletion of *rnc* also exhibited a slight decrease in cell length. This is noteworthy because it supports the hypothesis that a balance between the two factors, S15 and RNase III, is critical *in vivo*. Because S15 and RNase III have primary roles in maturation, it is also likely that changes in cell division and growth rate are secondary effects of improperly or decreased mature ribosomes. Further investigation is required to confirm this hypothesis.

It has been previously demonstrated that the impairment of RNase III activity suppresses cold-sensitive mutants of *nus* transcription factors [49]. This study suggests that the absence of RNase III might allow proper folding of the precursor 16S rRNA transcript in *nus* mutants where transcription and processing of rRNA is already delayed [49]. This supports our hypothesis that slowing rRNA processing in the absence of RNase III could support multiple pathways of SSU maturation, especially in conditions where biogenesis is hindered. This is further corroborated by the growth data in Figure 4.C, in which the presence of exogenous RNase III leads to growth defects at 37°C but not at 25°C. Therefore, we speculate that *rnc* deletion allows diversification of pathways leading to 30S subunit maturation in a *rpsO* deletion strain.

It is well established that the incorporation of pre-16S rRNA in translating ribosomes is associated with decreased fidelity [50]. Although there is evidence of gate-keeper factors

that prevent this incorporation [51–53], it remains unclear what mechanism regulates the inclusion or exclusion of pre16S rRNA-containing 30S subunits into the 70S ribosomes. Here we detected immature 17S rRNA (in *ΔrpsO*) and 17S* rRNA (*ΔrncΔrpsO*) that can be incorporated into 70S-like ribosomes (Figure 7). It is likely that 70S ribosomes containing mature 16S rRNA, and not 17S* rRNA, in *ΔrncΔrpsO* are crucial for improved growth, relative to *ΔrpsO*; however, this remains to be fully established. Understanding the dynamics and importance of these different 16S rRNA forms is also critical to further understanding gate-keeper mechanisms. The identification of new, functionally interacting partners in ribosome biogenesis such as the one described in this paper brings us one step closer to understanding pathways of pre-30S SSU intermediates.

4. Materials and Methods:

4.1. Strains, plasmids, and Growth conditions

The S15 deletion strain, *ΔrpsO* in *E. coli* BW25113 was obtained from the KEIO collection [54]. The *ΔrpsO::kan* knockout in the W3110 background was constructed by the insertion of a kanamycin cassette into the *rpsO* ORF using P1 transduction [28]. The RNase III deletion strain contained a chloramphenicol maker in the MG1655 *E. coli* strain replacing the *rnc* gene (*Δrnc::cat*) and was a kind gift from Dr. Graham C. Walker. The double deletion (*ΔrpsOΔrnc*) was created by P1 transduction of the kanamycin and chloramphenicol knockout cassettes containing complete deletion of the reading frames of *rpsO* and *rnc* respectively, into W3110 (used in the majority of growth analyses and Figure 2) and BW25113 (used in experiments for rRNA analysis and cell length measurements in Figure 5 and 6) backgrounds. The replacement of the target areas in the chromosome, with the appropriate cassette, were verified by PCR with primers designed to confirm the absence of the *rpsO* and *rnc* genes. For complementation studies, pBAD-*rpsO* and pBAD-*rnc* were generated by cloning the ORF of each gene using restriction sites (NcoI and XbaI) into a pBAD/His vector from Invitrogen. Both proteins were expressed from an arabinose-inducible promoter and 0.2% arabinose was used to induce gene expression. Serial dilutions of log-phase, plasmid-borne cultures were spotted on LB agar containing 100 μg/mL ampicillin and 0.2% arabinose. An empty vector (pBAD/His) was used as control in these growth experiments (Figure 4.C). For comparison of growth under pBAD-*rnc* expression, the LB plates were grown for 48 hours at 25°C. For all liquid growth studies, all cultures were grown with agitation in LB broth without antibiotic (ampicillin) except for plasmid maintenance. Three growth experiments were performed for each strain and condition. The starting A_{600} for each culture, in each experiment, was ~0.02. Growth was measured in 96 well plates at 25°C and 37°C using a BioscreenC (Growth Curves, USA) and readings were taken every hour. We observed increased lysis of *ΔrpsO* cultures (of 100mL or more) when grown at 200 rpm or higher. Hence, we reduced the shaker rate to 170 rpm for cultures grown for harvesting. The liquid growth study for plasmid borne expression of RNase III and S15 were done at 28°C (Figure S7) because we wanted a slightly more robust growth to observe any complementation. The growth data were analyzed and plotted using Graphpad Prism. Each growth curve data point for growth data in Figure S7 is the average of three O.D measurements. The growth curves in Figure 2.A and 4.B have been plotted with standard

deviation as error bars. For ribosome isolation, cell growth was stopped at ~A_{600}= 0.4 by the addition of ice to the cultures after which the cells were pelleted and frozen at −80°C.

4.2. Sucrose Gradient Fractionation of Ribosomes

Frozen cell pellets (see above) were resuspended and lysed as previously described [13, 52]. After lysis, equivalent amounts of the cleared lysates were loaded onto 10-40% sucrose gradients [52] containing 50mM Tris-HCl (pH 7.8), 10mM $MgCl_2$ and 100mM KCl. Ribosomal peaks (30S, 50S, and 70S) were separated by centrifugation (Beckman SW-41 rotor) at 25,000 rpm, 4°C for 16 hrs. The sucrose gradients were analyzed using a Biocomp Piston Gradient Fractionator and Biocomp Model 251 Gradient Profiler. Ribosomal RNA concentrations were measured in real-time using a Bio-Rad Econo UV Monitor. The profiles were analyzed using Image J to calculate the area under the peaks. The peaks were labeled end-to-end for consistency and area for each peak was calculated. The area was represented as a fraction of total (all peak areas for each sample) and plotted as bar graphs. Three biological replicates were used in the analysis and standard deviation was calculated. A Welch's unpaired t-test was done to determine significance in differences between strains [38].

4.3. RNA Isolation and analysis:

The rRNA from three peak fractions (*ΔrpsO* in Figure 2.B) was analyzed by northern blot (1, 2, 3), where fraction 2 represents the top of the peak and fractions 1 and 3 were collected on either side of the peak (Figure S3). Ribosomal RNA was purified by Phenol/Chloroform extraction as described [55] and subject to northern blotting. Samples of rRNA were separated using 2% denaturing formaldehyde/agarose gels (25 cm. gel length) run at 60 V for 16 hours using a peristaltic pump to circulate running buffer. After electrophoresis, agarose gels were soaked in 0.5X TBE for 30 min. The gels were then blotted onto GeneScreen Plus (PerkinElmer) using a BioRad Trans-Blot SD Semi-Dry Electrophoretic Transfer Cell at a power setting of 3 mA/cm^2 for 30 min. After transfer, blots were blocked in ULTRAhyb-Oligo Buffer (Applied Biosystems) for 1 hour in a Hybaid H-9360 hybridization oven set at 42°C. Probes were made using oligonucleotides specific to sequences in either the mature 16S RNA (5′-CGCATTTCACCGCTACA-3′), 5′ leader – 5′-CGTGTTCACTCTTGAGACTTGG-3′ or 3′ trailer - 5′-CAAAGTACGCTTCTTTAAG-3′.

Probes were ^{32}P end labelled (200 pmols in 40 μL) using T4 Polynucleotide Kinase (New England Biolabs). Oligonucleotides were heated at 64°C for 5 min. and then chilled prior to the addition of 5 μL T4 PNK Buffer, 100 uCi γ P^{32} ATP and 2 μL of T4 Polynuclotide Kinase. Labeling reactions were done at 37°C for 20 min. after which they were incubated at 65°C for 20 min. to stop the reaction. Unincorporated P^{32} was removed using a BioRad Micro Bio-Spin Chromatography Column.

For analysis of the northern blots (see above), the area of each band at the 16S rRNA and 17S rRNA position was calculated using Image J. The area for three 30S subunit fractions (1,2,3) were summed for each sample and represented the band intensity for that sample. For example, all three fractions displayed 17S band in the *ΔrpsO* 25°C sample. The three band areas were calculated separately and summed. The band intensities from each blot

(16S rRNA probe, 17S rRNA leader probe, and 17S rRNA trailer probe) were normalized separately by using the *wild-type* 37°C sample as base-line=1. The other three samples wild-type 25°C, *ΔrpsO* 37°C, and *ΔrpsO* 25°C are represented as a fraction of 1 and the data provided as three graphs in Figure 2.C. In Figure S5, the band intensities were calculated using Image J. The band intensity was measured for each band and presented as a percent of total band intensity for the lane.

4.4. RNA analysis by 3'-5' RACE

The rRNA from the 30S subunits as well as 70S ribosomal fractions from all strains were analyzed by modified 3'-5' RACE. The *wild-type* and *Δrnc* were compared in Figure 3; distinct 30S and 70S populations were collected as shown in Figure 3.A. For comparison of *ΔrpsO* and the double deletion (*ΔrpsOΔrnc*, four separate fractions were collected as denoted in Figure 6.A. Modified 3-'5' RACE was performed as described [13, 20]. 200ng of purified RNA was used for initial circularization with T4 RNA ligase (NEB) overnight at 16°C. Reverse transcription was done using AMV reverse transcriptase (NEB) for 60 minutes followed by PCR amplification. The modification to the protocol includes two heat denaturation steps – one carried out at 74°C and quickly cooled before ligation, and another after reverse transcription (74°C for 15 minutes). The RACE PCR products were gel purified using gel band purification kit from GE Healthcare, ligated into pCR 2.1 vector, and subcloned using TOPO-TA cloning kit (ThermoFischer Scientific). For each sample, plasmids were isolated and sequenced (Genewiz) from 10-12 transformed colonies. The reverse and forward primers used in the PCR can amplify and detect mature and immature rRNA species (REV:5'-CGTTCGACTTGCATGTGTTAGGC-3') and FOR: 5'-GAAGTAGGTAGCTTAACCTTCGGGAG-3'). The PCR products were resolved using a 2.5 % agarose gel. The control bands for 17S* rRNA (361 bp), 17S rRNA (327bp), and 16S rRNA (179bp) species were collected from RACE experiments where the PCR product was gel-purified, TOPO cloned, and sequenced. These DNA products were used as marker in Figure 3.B.

4.5. Mass spectrometry:

The SSUs from wild-type and *ΔrpsO* cultures grown at two temperature conditions (25°C and 37°C) were isolated from sucrose gradients. The samples were normalized for RNA concentration (at 100 ng/μL) and mixed in SDS-PAGE gel loading dye [55]. To remove sucrose prior to mass spec, the RNP samples were loaded on a 13% SDS-PAGE gel and run until a band was resolved just below the well for each sample. For each sample, the bands were excised and then the gel slabs treated with trypsin and the resulting peptides were injected onto a Q Exactive Plus mass spectrometer connected to an Easy nLC1000 (Thermo Fisher – University of Rochester Mass Spectrometry Resource Laboratory https://www.urmc.rochester.edu/research/mass-spectrometry.aspx). Data dependent acquisition (DDA) was employed to isolate and fragment precursor ions. The resulting data were analyzed using Proteome Discoverer 1.4 software (Thermo Fisher) using Mascot (Matrix Science). Percolator was used as the false discovery rate (FDR) calculator and peptides with a q-value greater than 0.01 were filtered out. Peptide spectral counts were used to report the relative the abundance of detected proteins. For each experiment, proteins detected with a false discovery rate (FDR) of less than 1% are listed in Supplementary Tables 1 and 2.

The raw data for the complete protein list is provided in Supplementary Table 1 and all ribonucleases are provided in Supplementary Table 2.

4.6. Cell length measurements:

Cells from four strains grown at 25°C (*wild-type, ΔrpsO, Δrnc* and *ΔrncΔrpsO)* were imaged using phase contrast microscopy. Samples were prepared by mounting a 2-5 liters of log-phase liquid cultures (LB media) on slides topped with coverslips. The 100X lens on the Nikon Eclipse E600 instrument was used to capture multiple regions of each sample slide. The cell length measurements were made using Image J using a measurement scale for each image. The data was analyzed in Excel and plotted using Graphpad Prism (version 8.3). For each strain, 100 measurements were averaged and plotted as a scatter plot in Figure 5.B. An unpaired t-test was done to determine significance in differences between strains.

Supplementary Material

Refer to Web version on PubMed Central for supplementary material.

ACKNOWLEDGEMENTS

We would like to thank Dr. Michael Welte for providing access to the microscope for cell length experiments, Dr. David Goldfarb for the BioscreenC, which was used for growth studies, and Dr. Sina Ghaemmaghami for helping us with mass spectrometry analyses. This work was supported by National Institutes of Health grant to G.M.C (GM62432).

Abbreviations

rRNA	ribosomal RNA
SSU	small subunit
LSU	large subunit
r-proteins	ribosomal proteins
RACE	Rapid amplification of cDNA ends

References:

1. Ramakrishnan V and White SW, Ribosomal protein structures: insights into the architecture, machinery and evolution of the ribosome. Trends Biochem Sci, 1998. 23(6): p. 208–12. [PubMed: 9644974]
2. Carter AP, et al. , Functional insights from the structure of the 30S ribosomal subunit and its interactions with antibiotics. Nature, 2000. 407(6802): p. 340–8. [PubMed: 11014183]
3. Comartin DJ and Brown ED, Non-ribosomal factors in ribosome subunit assembly are emerging targets for new antibacterial drugs. Curr Opin Pharmacol, 2006. 6(5): p. 453–8. [PubMed: 16890019]
4. Foster C and Champney WS, Characterization of a 30S ribosomal subunit assembly intermediate found in Escherichia coli cells growing with neomycin or paromomycin. Arch Microbiol, 2008. 189(5): p. 441–9. [PubMed: 18060665]
5. Maguire BA, Inhibition of bacterial ribosome assembly: a suitable drug target? Microbiol Mol Biol Rev, 2009. 73(1): p. 22–35. [PubMed: 19258531]

6. Siibak T and Remme J, Subribosomal particle analysis reveals the stages of bacterial ribosome assembly at which rRNA nucleotides are modified. RNA, 2010. 16(10): p. 2023–32. [PubMed: 20719918]
7. Bjorkman J, et al. , Novel ribosomal mutations affecting translational accuracy, antibiotic resistance and virulence of Salmonella typhimurium. Mol Microbiol, 1999. 31(1): p. 53–8. [PubMed: 9987109]
8. Champney WS, The other target for ribosomal antibiotics: inhibition of bacterial ribosomal subunit formation. Infect Disord Drug Targets, 2006. 6(4): p. 377–90. [PubMed: 17168803]
9. Deutscher MP, Maturation and degradation of ribosomal RNA in bacteria. Prog Mol Biol Transl Sci, 2009. 85: p. 369–91. [PubMed: 19215777]
10. Shajani Z, Sykes MT, and Williamson JR, Assembly of bacterial ribosomes. Annu Rev Biochem, 2011. 80: p. 501–26. [PubMed: 21529161]
11. Sykes MT, et al. , Quantitative proteomic analysis of ribosome assembly and turnover in vivo. J Mol Biol, 2010. 403(3): p. 331–45. [PubMed: 20709079]
12. Earnest TM, et al. , Toward a Whole-Cell Model of Ribosome Biogenesis: Kinetic Modeling of SSU Assembly. Biophys J, 2015. 109(6): p. 1117–35. [PubMed: 26333594]
13. Gupta N and Culver GM, Multiple in vivo pathways for Escherichia coli small ribosomal subunit assembly occur on one pre-rRNA. Nat Struct Mol Biol, 2014. 21(10): p. 937–43. [PubMed: 25195050]
14. Smith BA, et al. , Characterization of 16S rRNA Processing with Pre-30S Subunit Assembly Intermediates from E. coli. J Mol Biol, 2018. 430(12): p. 1745–1759. [PubMed: 29660326]
15. Nikolaev N, Glazier D, and Schlessinger D, Cleavage by ribonuclease III of the complex of 30 S pre-ribosomal RNA and ribosomal proteins of Escherichia coli. J Mol Biol, 1975. 94(2): p. 301–4. [PubMed: 1095771]
16. Young RA and Steitz JA, Complementary sequences 1700 nucleotides apart form a ribonuclease III cleavage site in Escherichia coli ribosomal precursor RNA. Proc Natl Acad Sci U S A, 1978. 75(8): p. 3593–7. [PubMed: 358189]
17. Cheng ZF and Deutscher MP, Quality control of ribosomal RNA mediated by polynucleotide phosphorylase and RNase R. Proc Natl Acad Sci U S A, 2003. 100(11): p. 6388–93. [PubMed: 12743360]
18. Davies BW, et al. , Role of Escherichia coli YbeY, a highly conserved protein, in rRNA processing. Mol Microbiol, 2010. 78(2): p. 506–18. [PubMed: 20807199]
19. Jain C, RNase AM, a 5′ to 3′ exonuclease, matures the 5′ end of all three ribosomal RNAs in E. coli. Nucleic Acids Res, 2020. 48(10): p. 5616–5623. [PubMed: 32343306]
20. Al Refaii A and Alix JH, Ribosome biogenesis is temperature-dependent and delayed in Escherichia coli lacking the chaperones DnaK or DnaJ. Mol Microbiol, 2009. 71(3): p. 748–62. [PubMed: 19054328]
21. Gan J, et al. , Structural insight into the mechanism of double-stranded RNA processing by ribonuclease III. Cell, 2006. 124(2): p. 355–66. [PubMed: 16439209]
22. Macrae IJ, et al. , Structural basis for double-stranded RNA processing by Dicer. Science, 2006. 311(5758): p. 195–8. [PubMed: 16410517]
23. Cukras AR and Green R, Multiple effects of S13 in modulating the strength of intersubunit interactions in the ribosome during translation. J Mol Biol, 2005. 349(1): p. 47–59. [PubMed: 15876367]
24. Jagannathan I and Culver GM, Assembly of the central domain of the 30S ribosomal subunit: roles for the primary binding ribosomal proteins S15 and S8. J Mol Biol, 2003. 330(2): p. 373–83. [PubMed: 12823975]
25. Tobin C, et al. , Ribosomes lacking protein S20 are defective in mRNA binding and subunit association. J Mol Biol, 2010. 397(3): p. 767–76. [PubMed: 20149799]
26. Mizushima S and Nomura M, Assembly mapping of 30S ribosomal proteins from E. coli. Nature, 1970. 226(5252): p. 1214. [PubMed: 4912319]
27. Hase Y, et al. , Impairment of ribosome maturation or function confers salt resistance on Escherichia coli cells. PLoS One, 2013. 8(5): p. e65747. [PubMed: 23741511]

28. Bubunenko M, et al. , 30S ribosomal subunits can be assembled in vivo without primary binding ribosomal protein S15. RNA, 2006. 12(7): p. 1229–39. [PubMed: 16682557]
29. Britton RA, Role of GTPases in bacterial ribosome assembly. Annu Rev Microbiol, 2009. 63: p. 155–76. [PubMed: 19575570]
30. Nomura M, Bacterial ribosome. Bacteriol Rev, 1970. 34(3): p. 228–77. [PubMed: 16350216]
31. King TC and Schlessinger D, S1 nuclease mapping analysis of ribosomal RNA processing in wild type and processing deficient Escherichia coli. J Biol Chem, 1983. 258(19): p. 12034–42. [PubMed: 6311836]
32. Gegenheimer P and Apirion D, Processing of rRNA by RNAase P: spacer tRNAs are linked to 16S rRNA in an RNAase P RNAase III mutant strain of E. coli. Cell, 1978. 15(2): p. 527–39. [PubMed: 363277]
33. Mangiarotti G, et al. , Role of precursor 16S RNA in assembly of E. coli 30S ribosomes. Nature, 1975. 253(5492): p. 569–71. [PubMed: 1090843]
34. Akanuma G, et al. , Inactivation of ribosomal protein genes in Bacillus subtilis reveals importance of each ribosomal protein for cell proliferation and cell differentiation. J Bacteriol, 2012. 194(22): p. 6282–91. [PubMed: 23002217]
35. Song W, et al. , Antibiotic stress-induced modulation of the endoribonucleolytic activity of RNase III and RNase G confers resistance to aminoglycoside antibiotics in Escherichia coli. Nucleic Acids Res, 2014. 42(7): p. 4669–81. [PubMed: 24489121]
36. Naganathan A and Moore SD, Crippling the essential GTPase Der causes dependence on ribosomal protein L9. J Bacteriol, 2013. 195(16): p. 3682–91. [PubMed: 23772068]
37. Sayed A, Matsuyama S, and Inouye M, Era, an essential Escherichia coli small G-protein, binds to the 30S ribosomal subunit. Biochem Biophys Res Commun, 1999. 264(1): p. 51–4. [PubMed: 10527840]
38. Sawilowsky SS, <Fermat Schubert Einstein and Behrens-Fisher_ The Probable Diff.pdf>. Journal of Modern Applied Statistical Methods, 2002. 1(2): p. 461–472.
39. Travers AA, Conserved features of coordinately regulated E. coli promoters. Nucleic Acids Res, 1984. 12(6): p. 2605–18. [PubMed: 6369249]
40. Besancon W and Wagner R, Characterization of transient RNA-RNA interactions important for the facilitated structure formation of bacterial ribosomal 16S RNA. Nucleic Acids Res, 1999. 27(22): p. 4353–62. [PubMed: 10536142]
41. Korostelev A, et al. , Interactions and dynamics of the Shine Dalgarno helix in the 70S ribosome. Proc Natl Acad Sci U S A, 2007. 104(43): p. 16840–3. [PubMed: 17940016]
42. Dennis PP, Russell AG, and Moniz De Sa M, Formation of the 5′ end pseudoknot in small subunit ribosomal RNA: involvement of U3-like sequences. RNA, 1997. 3(4): p. 337–43. [PubMed: 9085841]
43. Court DL, et al. , RNase III: Genetics and function; structure and mechanism. Annu Rev Genet, 2013. 47: p. 405–31. [PubMed: 24274754]
44. Byrgazov K, Vesper O, and Moll I, Ribosome heterogeneity: another level of complexity in bacterial translation regulation. Curr Opin Microbiol, 2013. 16(2): p. 133–9. [PubMed: 23415603]
45. Guthrie C, Nashimoto H, and Nomura M, Structure and function of E. coli ribosomes. 8. Cold-sensitive mutants defective in ribosome assembly. Proc Natl Acad Sci U S A, 1969. 63(2): p. 384–91. [PubMed: 4895536]
46. Forchhammer J and Lindahl L, Growth rate of polypeptide chains as a function of the cell growth rate in a mutant of Escherichia coli 15. J Mol Biol, 1971. 55(3): p. 563–8. [PubMed: 4927947]
47. Dai X and Zhu M, Coupling of Ribosome Synthesis and Translational Capacity with Cell Growth. Trends Biochem Sci, 2020. 45(8): p. 681–692. [PubMed: 32448596]
48. Bakshi S, et al. , Superresolution imaging of ribosomes and RNA polymerase in live Escherichia coli cells. Mol Microbiol, 2012. 85(1): p. 21–38. [PubMed: 22624875]
49. Bubunenko M, et al. , Nus transcription elongation factors and RNase III modulate small ribosome subunit biogenesis in Escherichia coli. Mol Microbiol, 2013. 87(2): p. 382–93. [PubMed: 23190053]

50. Roy-Chaudhuri B, Kirthi N, and Culver GM, Appropriate maturation and folding of 16S rRNA during 30S subunit biogenesis are critical for translational fidelity. Proc Natl Acad Sci U S A, 2010. 107(10): p. 4567–72. [PubMed: 20176963]

51. Connolly K and Culver G, Overexpression of RbfA in the absence of the KsgA checkpoint results in impaired translation initiation. Mol Microbiol, 2013. 87(5): p. 968–81. [PubMed: 23387871]

52. Connolly K, Rife JP, and Culver G, Mechanistic insight into the ribosome biogenesis functions of the ancient protein KsgA. Mol Microbiol, 2008. 70(5): p. 1062–75. [PubMed: 18990185]

53. Jacob AI, et al. , Conserved bacterial RNase Ybe Y plays key roles in 70S ribosome quality control and 16S rRNA maturation. Mol Cell, 2013. 49(3): p. 427–38. [PubMed: 23273979]

54. Baba T, et al. , Construction of Escherichia coli K-12 in-frame, single-gene knockout mutants: the Keio collection. Mol Syst Biol, 2006. 2: p. 2006 0008.

55. Maniatis SF, Molecular Cloning - A laboratory manual Second edition. 1989.

56. Shen WF, Squires C, and Squires CL, Nucleotide sequence of the rrnG ribosomal RNA promoter region of Escherichia coli. Nucleic Acids Res, 1982. 10(10): p. 3303–13. [PubMed: 6285294]

Highlights:

- The absence of ribosomal protein S15 results in impaired ribosomal rRNA processing
- A novel precursor 16S rRNA accumulates in the absence of endoribonuclease RNase III
- Cold-sensitivity and cell elongation phenotypes are suppressed by deleting RNase III
- Altered incorporation of pre-16S rRNA in 70S points to a suppression mechanism

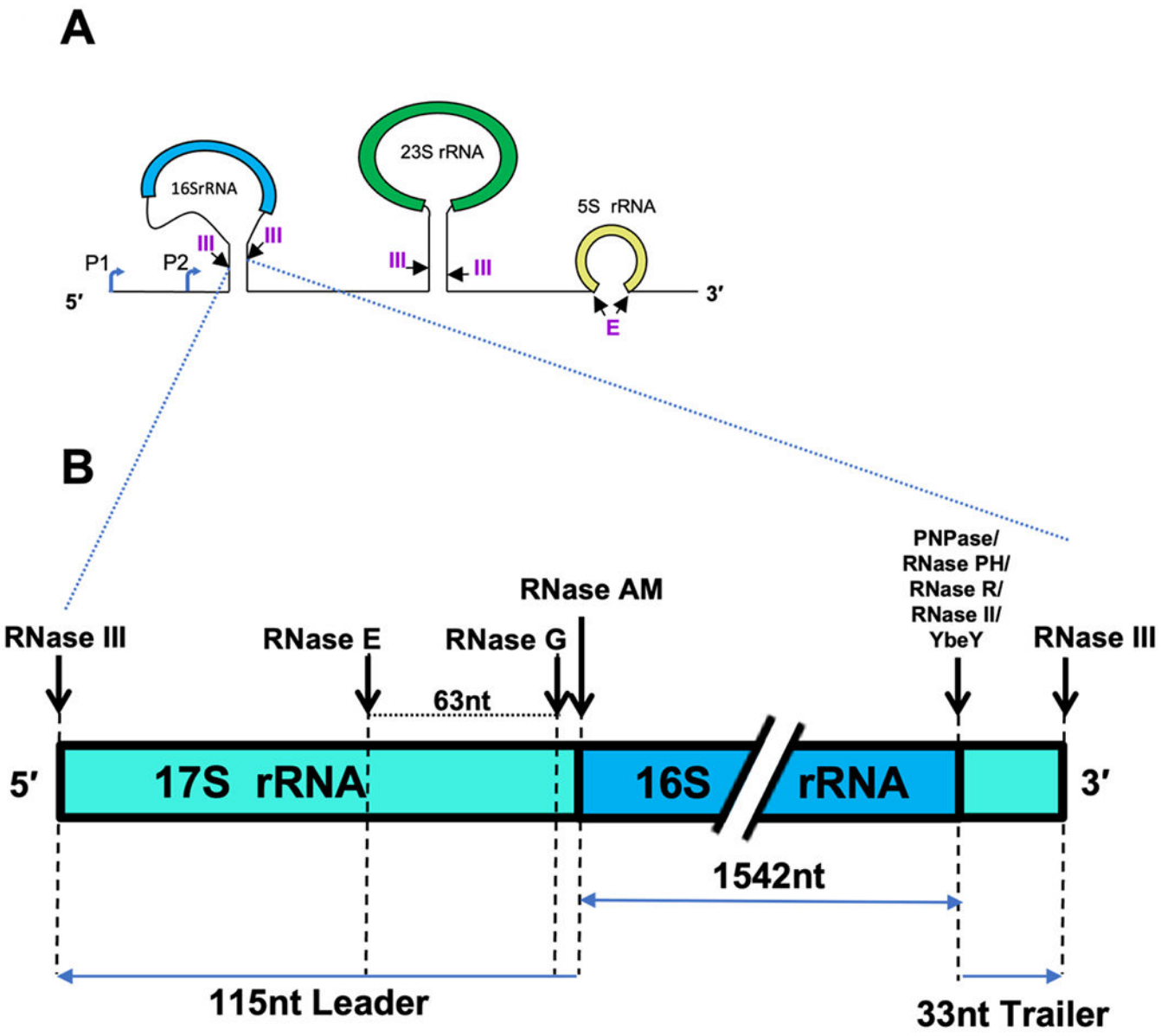

Figure 1: Schematic of 16S rRNA processing:

1.A) A schematic showing a generalized primary transcript of ribosomal RNA in *E. coli.* The mature regions (16S rRNA: *blue*, 23SrRNA: *green*, 5S rRNA:*yellow*) are flanked by precursor sequences that undergo subsequent processing by ribonucleases and are detailed in 1.B. Sites of action of enzymes, RNase III and E known to release pre-rRNA from the transcript are shown. P1 and P2 indicate alternative sites of transcription initiation (not drawn to scale).

1.B) A detailed representation of 16S rRNA and its flanking precursor sequences that result from RNase III cleavage is shown. 17S rRNA includes 16S rRNA (1542 nucleotides; *blue*) along with the leader (5′) and trailer (3’) sequences (*cyan*). The arrows depict the site of cleavage by nucleases that act during the maturation of 16S rRNA. RNase III cleaves the primary transcript to release 17S rRNA containing 115 nucleotides at the 5’ end and 33

nucleotides at the 3’ end. Endonucleases, RNase E and RNase G, and exonuclease, RNase AM further process the leader region. Several exonucleases (PNPase, RNase PH, RNase R, RNase II) and endonuclease, YbeY are implicated in the processing of the trailer region to form mature 16S rRNA.

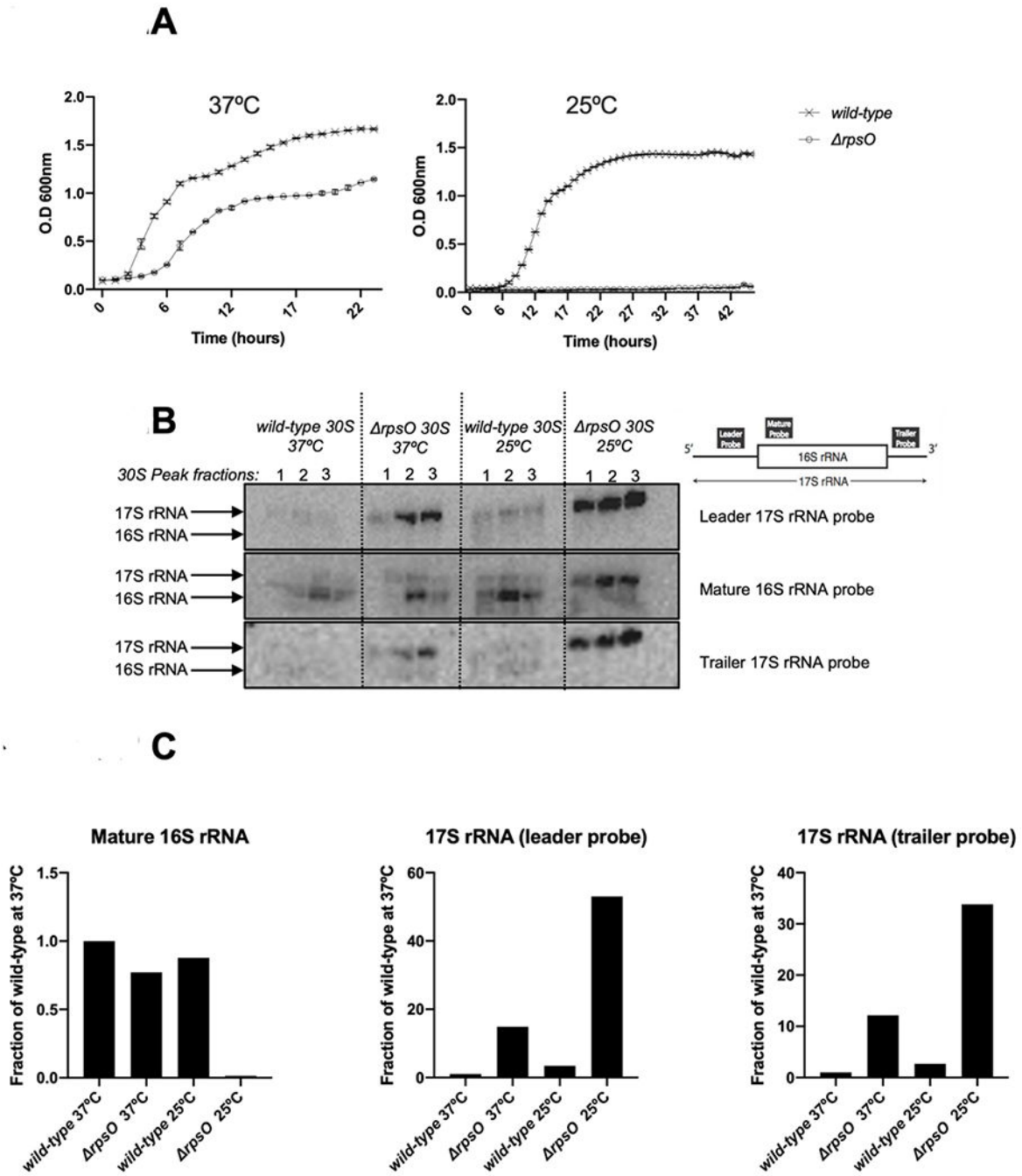

Figure 2: The absence of S15 severely impairs 16S rRNA maturation and causes ribosome deficiency.

2.A) Growth curves of *wild-type* (*cross marks*) and *ΔrpsO* (*open circles*) strains, grown at 37°C or 25°C. The X-axis indicates the average of three readings at A_{600} and the Y-axis indicates time (in hours). The error bars represent the standard deviation of three independent measurements.

2.B) The ribosomal RNA isolated from 30S subunits of *wild-type* and *ΔrpsO* grown at two temperature conditions (37°C and 25°C) were subjected to Northern blot analysis. The results of northern blots using three probes examine: Leader, 17S rRNA; mature, 16S rRNA:

and Trailer, 17S rRNA as shown. Three fractions isolated from free SSUs (see Figure S3) are shown here as 1,2, and 3. Two species are indicated in the blots – the top band is 17S rRNA and the bottom band is 16S rRNA. The inset in the top right corner of the blot indicates where the probes bind to detect either 16S or 17S rRNA. The presence of 17S rRNA is confirmed by leader and trailer probe binding in the higher molecular weight position (indicated by arrow).

2.C) Quantification of northern results shown in Figure 2.B. Image J was used to calculate band densities and area for the 16S rRNA and 17S rRNA bands. For each probe, the total band intensity of the three 30S peak fractions was normalized as a fraction of *wild-type* at 37°C (see Materials and Methods). The band intensity was normalized individually for each probe – 16S rRNA probe, 17S rRNA leader probe, and 17S rRNA trailer probe as shown here in three graphs. For each graph, the *wild-type* at 37°C sample was used as base-line (1) and the other samples (*wild-type* 25°C, *ΔrpsO* 37°C, and *ΔrpsO* 25°C) are represented as a fraction of 1.

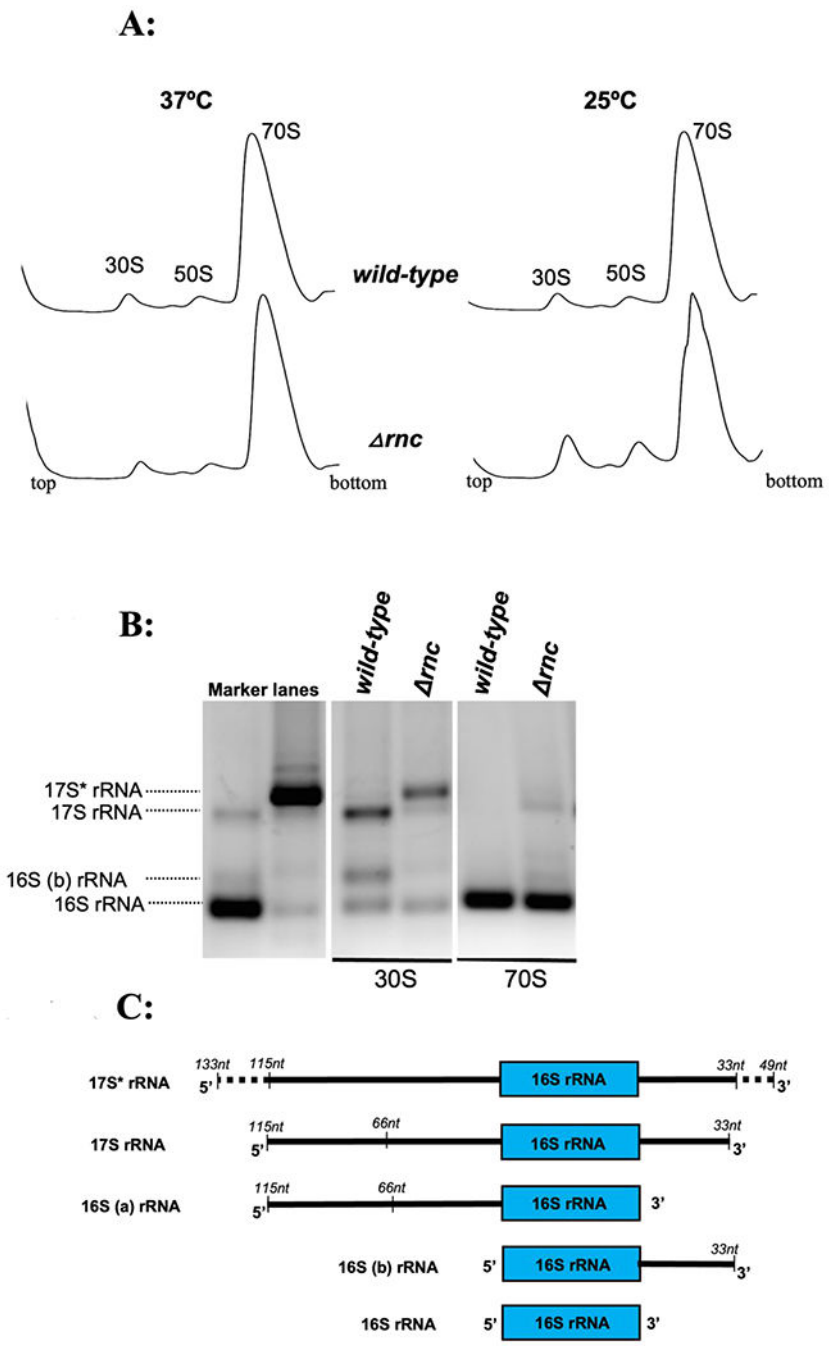

Figure 3: The deletion of RNase III results in the accumulation of a novel precursor rRNA processing intermediate

3.A) Sucrose gradient profile analyses of *wild-type* and *Δrnc* at 37°C and 25°C monitored at A_{254nm}. The 30S subunit, 50S subunit, and 70S ribosome peaks are indicated.

3.B) Modified 3'-5' RACE of rRNA from the 30S subunit and 70S ribosome fractions for *wild-type* and *Δrnc* grown at 25°C. Primers specific to the 16S rRNA sequence were used. The RACE products were separated and visualized on a 2.5 % agarose gel. The electrophoresis gel image is shown here with control bands for 16S rRNA and higher

molecular weight species (first two lanes). The control RACE products were obtained as described in Materials and Methods.

3.C) Schematic of modified 3'-5' RACE products shown in Figure 3.B. These species were identified by cloning and sequencing of the PCR products of different lengths as previously described [14]. It should be noted that the extensions for 17S* rRNA are not drawn to scale. The exact sequence is illustrated in Figure S8. The designations (a) and (b) indicate 16S rRNA that is completely processed at one end while still retraining precursor sequence at the other end. These designations are as previously described [13, 14].

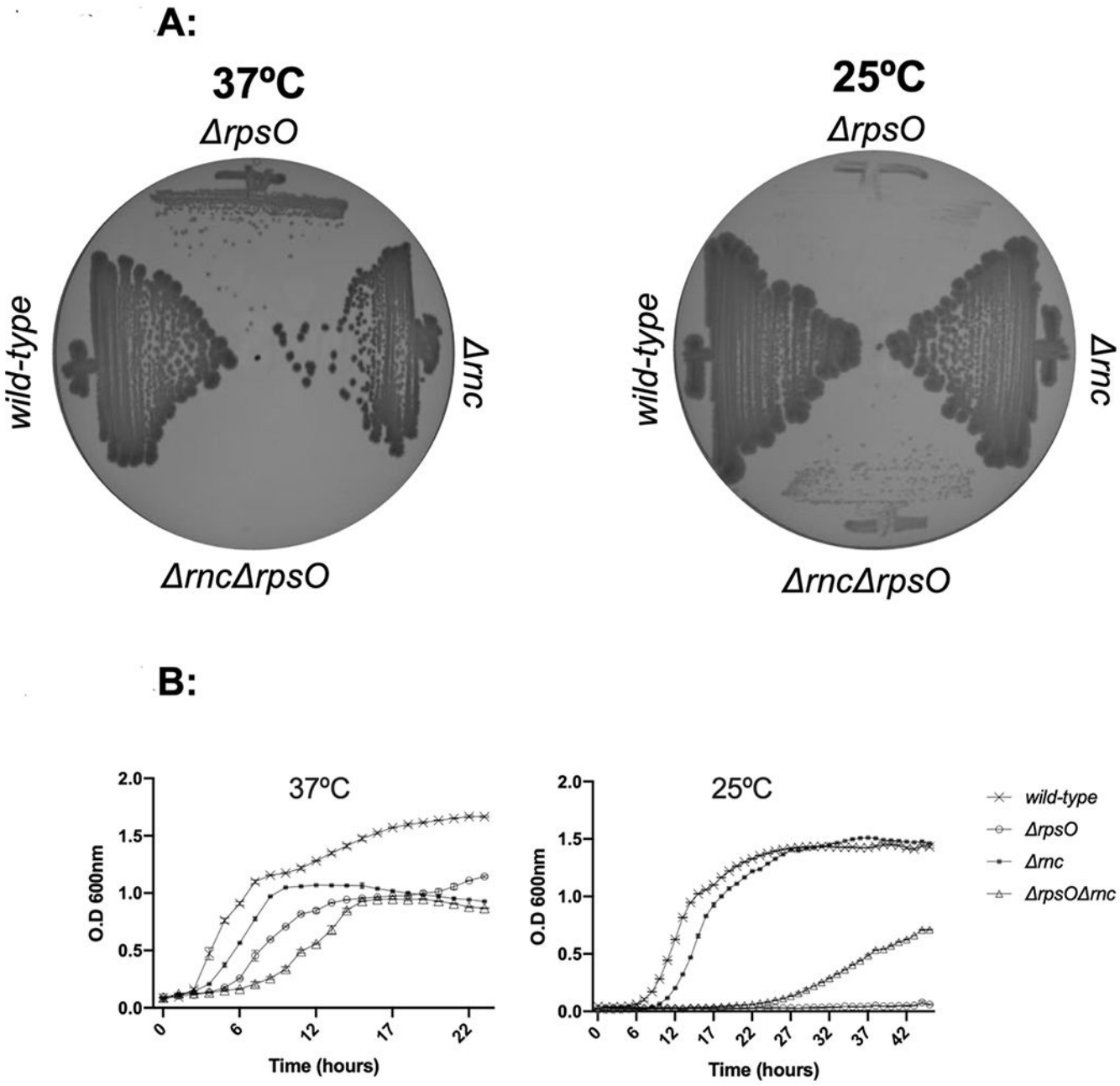

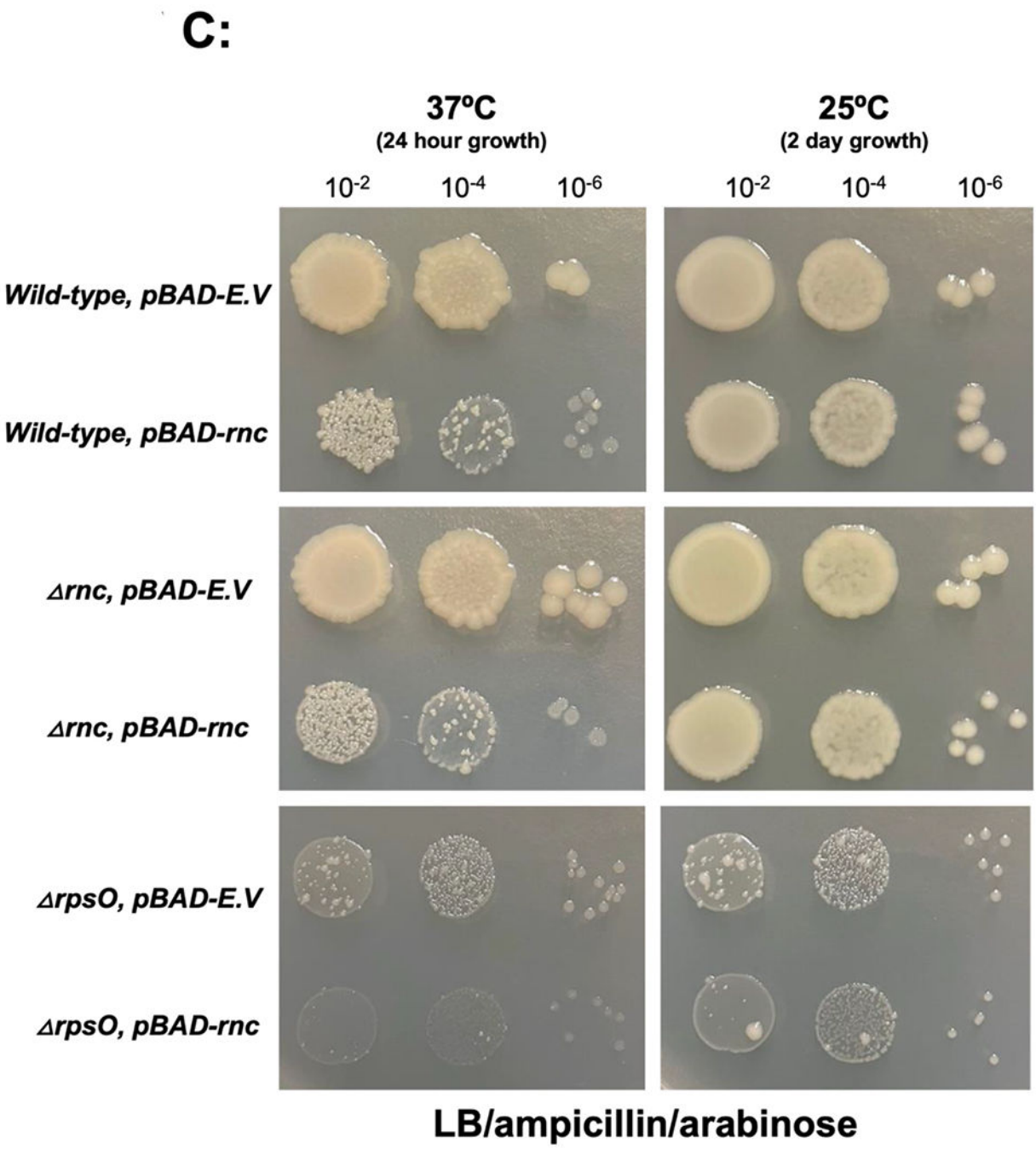

Figure 4: Cold sensitivity associated with deletion of *rpsO* is partially suppressed by co-deletion of *rnc*.

4.A) Growth on solid media at two temperatures reveals a synthetic interaction between *rnc* and *rpsO*. The gene coding for RNase III (*rnc*) was deleted from a *ΔrpsO* background and growth of four *allelic* strains (*wild-type*, *Δrnc*, *ΔrpsO*, and *ΔrncΔrpsO*) at 37°C (left plate) and 25°C (right plate) is compared in the *E. coli* background, W3110.

4.B) Growth profiles of four strains (*wild-type-cross* mark; *Δrnc*-closed squares; *ΔrpsO*-open circles; and *ΔrncΔrpsO*-open triangles) at 37°C (left) and 25°C (right) are shown. The

X-axis represents $O.D_{600}$ readings and the Y-axis represents time in hours. The average of three experiments and the calculated standard deviation is represented for each time point. 4.C) The effect of RNase III expression using arabinose-inducible plasmid (pBAD) reveals that cell growth is sensitive to RNase III levels. Strains containing either empty vector (*pBAD-E.V*) or the same vector designed for arabinose inducible expression of RNase III (*pBAD-rnc*) were grown in LB with ampicillin to early log-phase. Serial dilutions (10^{-2}, 10^{-4}, and 10^{-6}) were spotted on LB agar containing ampicillin (100μg/mL) and arabinose (0.2%) and grown overnight at either 37°C (left) and 25°C (right). The images of the plates were taken after 24 hours of growth for the 37°C condition and after 2-day growth for the 25°C condition.

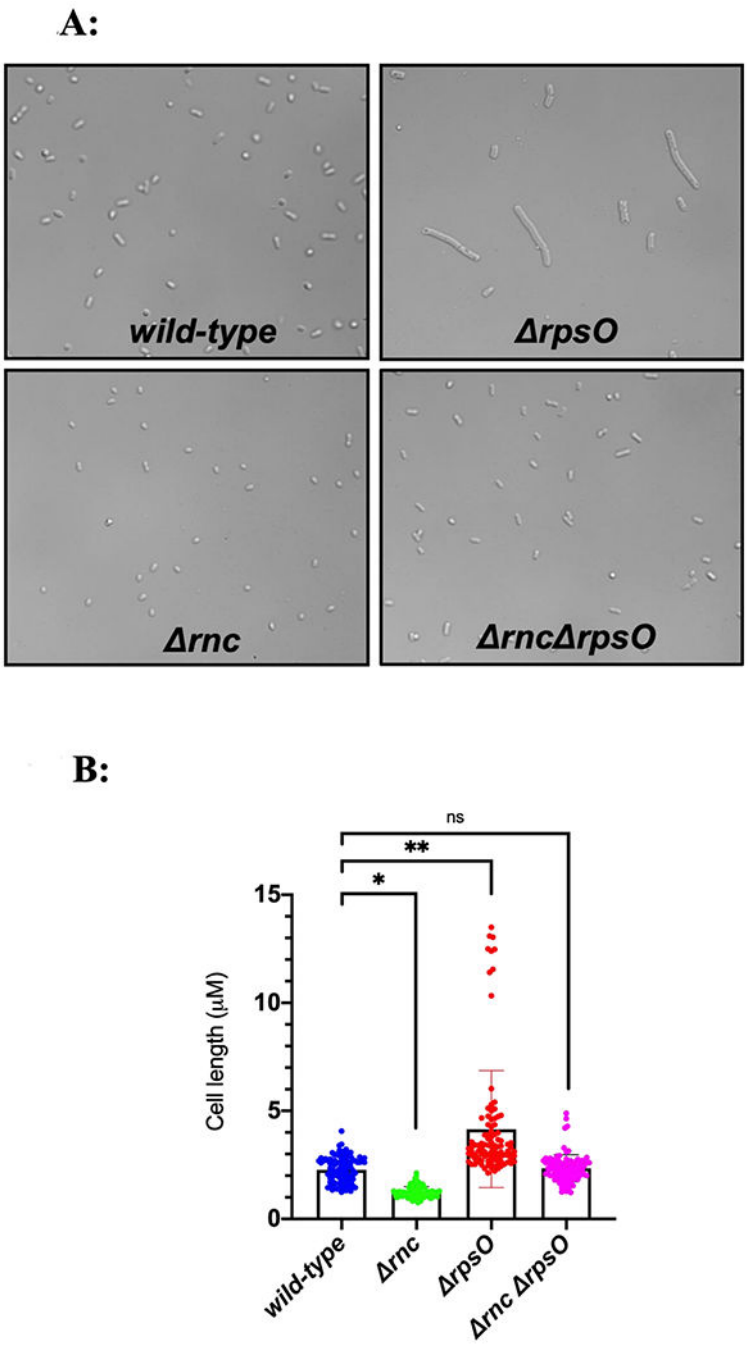

Figure 5: A cell elongation phenotype observed in Δ*rpsO* is suppressed by the deletion of *rnc* further supporting a functional interaction between these two loci.

5.A) Log-phase cultures of strains *wild-type*, *ΔrpsO*, *Δrnc*, and *ΔrncΔrpsO* grown at 25°C were visualized under a phase-contrast microscope. One representative micrograph for each strain is shown here.

5.B) Scatter blot representation of cell length measurements (100 cells/strain) for *wild-type*, *ΔrpsO*, *Δrnc*, and *ΔrncΔrpsO* grown at 25°C. The error bar is the standard deviation of the average of 100 measurements (see Materials and Methods). The four samples shown are: *wild-type* (blue), *Δrnc* (green,), *ΔrpsO* (red), and *ΔrncΔrpsO* (purple) with average cell

length of: 2.27 μm, 1.23 μm, 4.15 μm, and 2.34 μm respectively. The mean cell length of *wild-type* was significantly different (using an unpaired t-test) from *Δrnc* (* $p < .0001$) and from *μrpsO* (** $p<0.0001$). There was no significant difference in cell length between *wild-type* and *ΔrncΔrpsO* (ns $p=0.3935$).

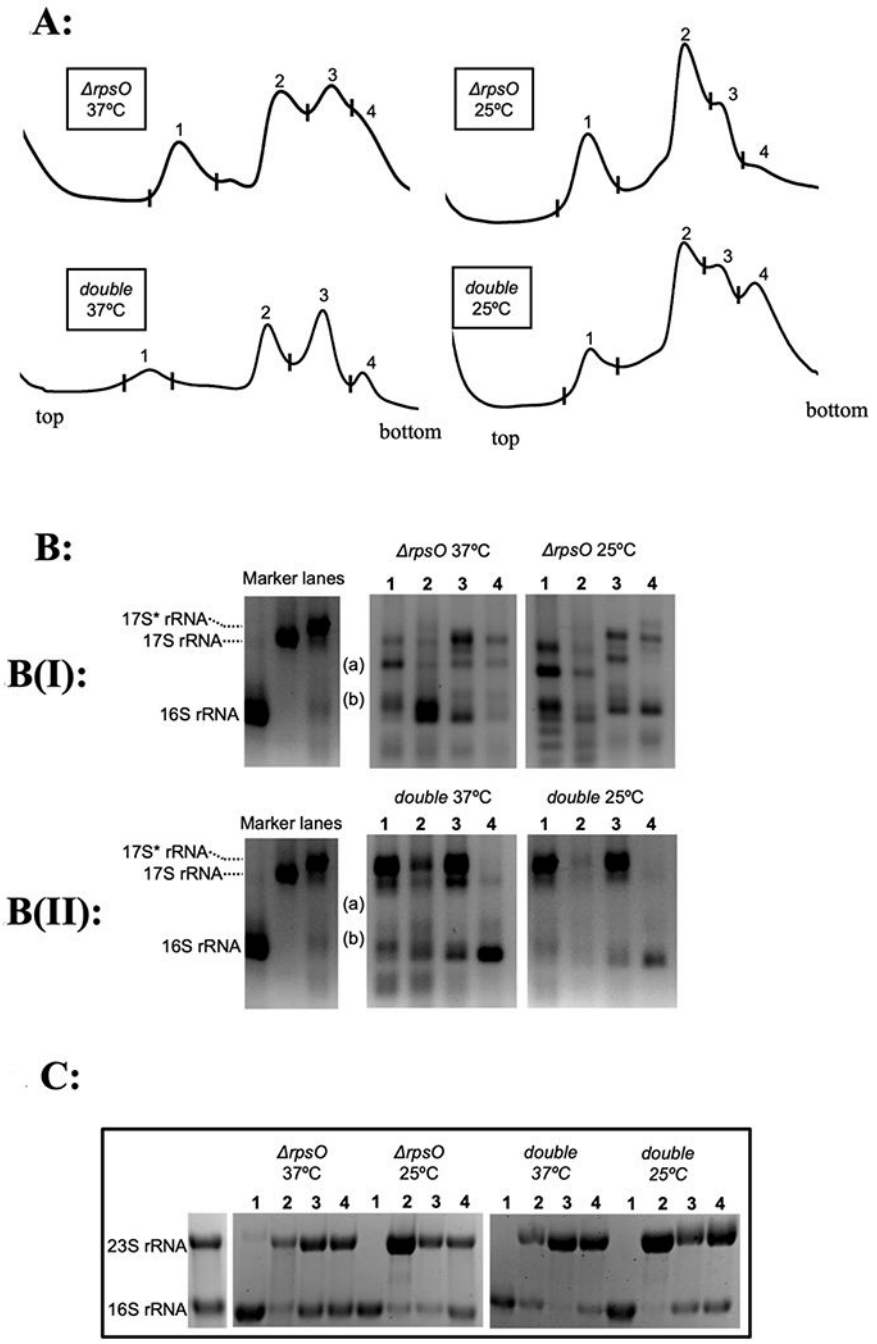

Figure 6: RNA analysis of Δ*rnc*Δ*rpsO* (double) reveals a population of 70S ribosomes containing predominantly mature 16S rRNA.

6.A) The sucrose gradient ribosome profiles of *ΔrpsO* and *ΔrncΔrpsO* (*double*) grown at 37°C and 25°C and measured at 254nm are shown. The sucrose gradient was fractionated into four samples as denoted by peaks 1 to 4.

6.B(I) and 6.B (II) Agarose gel electrophoresis images of modified 3'-5' RACE products generated from different sucrose gradient fractions (as numbered in 6.A). Figure 6.B(I) and 6.B (II) are analyses from *ΔrpsO* and *ΔrncΔrpsO*, respectively. Processing intermediates are shown in the schematic in Figure 3.C. The electrophoresis gel image is shown here with

control bands for 16S rRNA, 17S rRNA, and 17S* rRNA. (a) and (b) denote the pre-16S rRNA products (as shown in Figure 3.C), which are also identified by TOPO cloning and sequencing (Materials and Methods).

6.C) Total RNA isolated from the peaks (6.A) were run on a denaturing agarose gel to examine the rRNA content from all four fractionated peaks. 23S rRNA and 16S rRNA bands are marked by controls in the first lane.

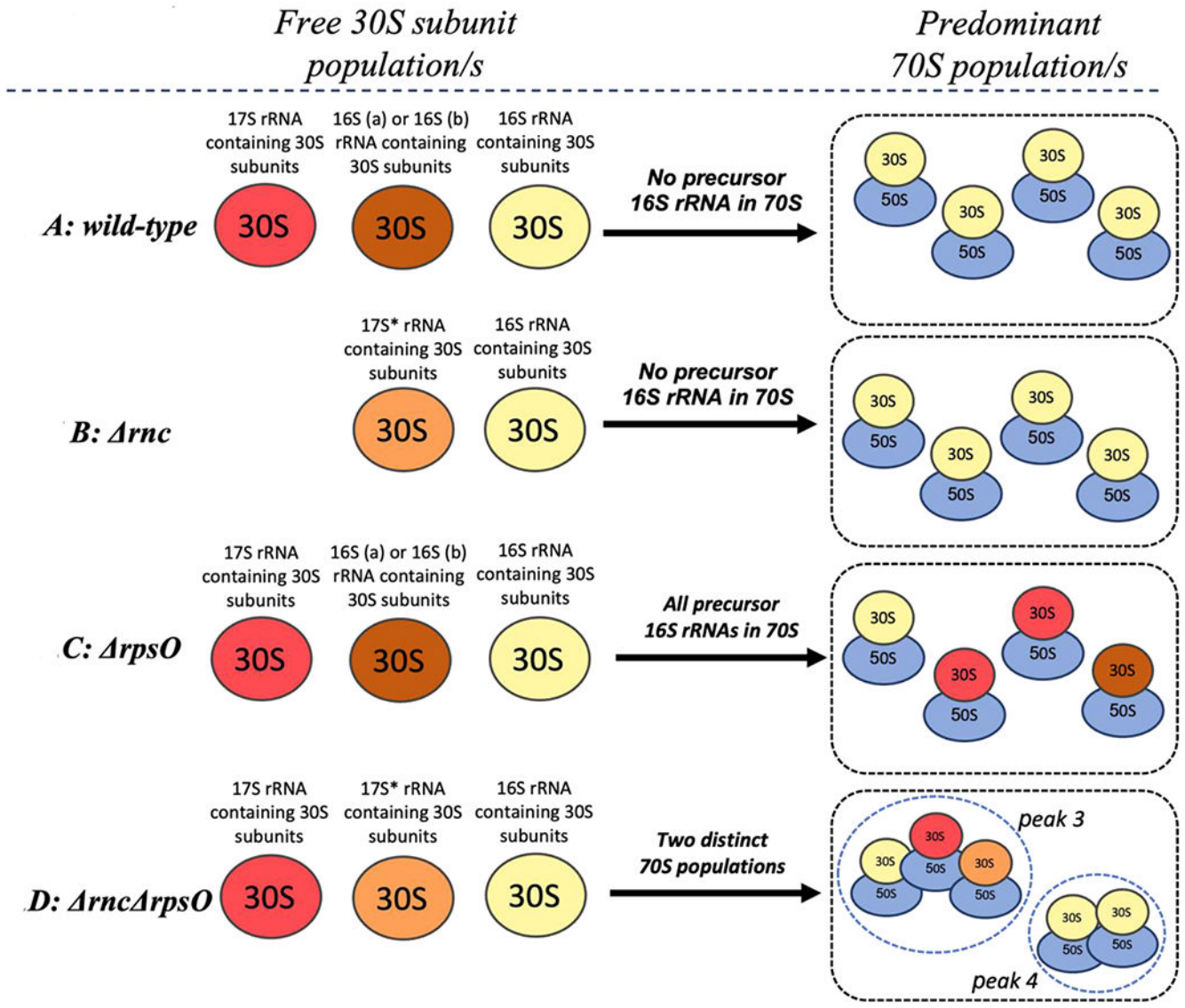

Figure 7: A summary of rRNA analysis from single deletions of *rpsO* and *rnc*, and the double deletion strain.

7.A) A wild-type strain contains a 70S peak representative of assembled 70S ribosomes with 30S subunits containing only mature 16S rRNA (*yellow*).

7.B) The deletion of *rnc* does not significantly impact processing. However, a precursor longer than 17S rRNA (called 17S* rRNA; *orange*) accumulates in free 30S subunits. The 17S* rRNA containing 30S subunits are not incorporated in the 70S fraction.

7.C) In the absence of *rpsO*, immature 16S rRNA, including 17S rRNA (*red*), 16S (a) and 16S (b) rRNA (*brown*) accumulates in both the free 30S subunits as well as 70S ribosomes. 30S subunits containing all immature rRNA can be detected in the assembled 70S peak.

7.D) When *rnc* is deleted from a *ΔrpsO* strain, the double deletion strain exhibits a second 70S peak that contains predominantly mature 16S rRNA. Two striking features of the double deletion strain are: 1) the presence of a longer 17S* rRNA as part of assembled 70S ribosomes, and 2) the 17S* rRNA is not incorporated in both 70S peaks. One population of

70S appears to contain mostly mature 16S rRNA. The two sub-populations of 70S particles are indicated by dotted circles and labeled peak 3 and peak 4 (as shown in Figure 6).